

Bistable Regimes in an Elastic Tensegrity System

Andrea Micheletti

Department of Civil Engineering and Computer Science Engineering
University of Rome Tor Vergata
Via Politecnico 1, 00133, Rome, Italy

micheletti@ing.uniroma2.it

This document is the preprint of the paper published on Proceedings of the Royal Society A, 8 June 2013, vol. 469 no. 2154 (<http://dx.doi.org/10.1098/rspa.2013.0052>).

Abstract

Tensegrity systems are prestressed frameworks composed by bars and cables. A particular elastic tensegrity system is examined. This system can be bistable in two fundamentally different ways, one depending on its geometric dimensions, and the other one depending on the initial deformation, or prestrain, of the elastic elements. A reduced-order semi-analytical model is derived, and its predictions are verified with a full-order numerical model. In particular, the critical geometry and prestrain at which the system switches from one regime to another are determined. This case study provides a benchmark and new insights on this class of structures.

Keywords: Elastic tensegrity system, bistability, benchmark

1 Introduction

A tensegrity structure is a pin-connected framework composed by bars and cables, with bars typically in compression, and cables necessarily in tension, such that the system is in a self-stressed state before the application of external loads.

Tensegrity systems have been considered for the first time in the 1948's by K. Snelson, when he was a student of R. B. Fuller. In the same period, D. G. Emmerich was also independently investigating structures of this kind. Starting in the 1960's, Snelson built several outdoor tensegrity sculptures, with bars never connected to each other. His term, "floating-compression", emphasizes this feature. Fuller instead used the words "tensile integrity" to highlight the fact that cables constitute a connected set. More details about the origin of tensegrities can be found in Gómez Jáuregui (2009).

Since the late 1970's, tensegrity systems have been rigorously studied by mathematicians in rigidity theory (Roth and Whiteley, 1981; Connelly, 1982), and by structural engineers (Calladine, 1978; Pellegrino and Calladine, 1986; Motro, 1992; Skelton and Sultan, 1997; Oppenheim and Williams, 1997), with steadily growing interest from the scientific community until present days. Due to their versatility and to their peculiar properties, applications for tensegrity structures have

been sought in many areas, especially in civil engineering, aerospace engineering, and robotics. Some representative references in these fields are: Rastorfer (1988); Motro (2003); Yuan et al. (2007); Skelton and de Oliveira (2009); Moored and Bart-Smith (2009); Zolesi et al. (2012); Paul et al. (2005); Shibata and Hirai (2009). Tensegrities are particularly suitable for variable geometry applications, such as deployable structures or adaptive systems, elements of which can be used as sensor or actuators. In addition, tensegrity systems possess a highly nonlinear mechanical behavior (Oppenheim and Williams, 2000, 2001; Michielsen et al., 2012), which can be exploited for designing new materials (Fraternali et al., 2012).

We focus on an aspect which is seldom examined in the literature, namely, the property of a tensegrity structure of being bistable or multistable. In the literature on tensegrities, the first occurrence of a bistable system appeared in Calladine (1978), as the classic two-bar system exhibiting snap-through instability. In cases like this, it occurs that by exchanging cables with bars, the energy passes from having a single well to having a double well. A more significative example has been given by Defossez (2003), who reported the case of an elastic tensegrity structure with multiple stable equilibrium configurations. Ranganathan et al. (2005) showed that the classic tensegrity prisms can pass from one configuration to another with opposite orientation, if large elastic deformations of its members are allowed. In the same paper, other cases were also presented. More recently, Xu and Luo (2010) found multiple equilibrium configurations for various tensegrity systems. In Zhang et al. (2011) another tensegrity system which can have more than one equilibrium configuration has been presented.

In the present study, we analyze a particular structure (Fig. 1) which can pass from one to two stable equilibrium configurations, either by a change in the overall geometry of the system, or by a change of prestrain, i.e. the initial deformation associated with the self-stress in the system. In

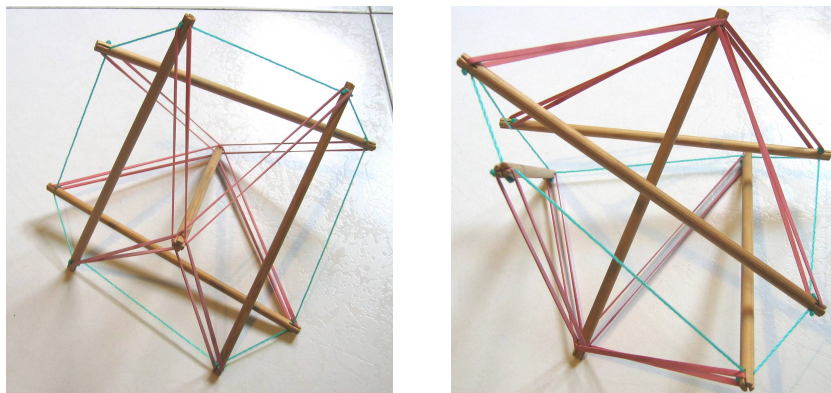


Figure 1: Two views of a dowel-and-string model of the tensegrity structure analyzed in this paper.

the next section, we review the basic definitions and notions about tensegrity systems that we need in order to perform our computations. In the third section, we present the actual analysis of the bistable structure.

2 Preliminaries

We first introduce the basic notions of selfstress and mechanism for frameworks, which are independent of constitutive assumptions. Then we briefly review the notions of stiffness and stability which

are usually employed for tensegrity systems. Many of the statements we make will be justified in the last subsection, where we present the detailed elastic formulation employed in the successive analysis.

2.1 Frameworks, selfstresses and mechanisms

A *framework* is defined as a set \mathcal{N} of N points, called *nodes*, in the three-dimensional Euclidean space, together with a set \mathcal{E} of E *edges* connecting pairs of nodes. We will say that $IJ \in \mathcal{E}$ is the edge connecting nodes $I, J \in \mathcal{N}$. Let \mathbf{p}_I be the position vector of node I with respect to a certain reference frame. The *configuration* of a framework is given by the $3N$ -dimensional vector \mathbf{p} which groups together all the nodal position vectors. Similarly, we can associate with each node a load vector and a displacement vector, so that \mathbf{f} and \mathbf{u} are the $3N$ -dimensional vectors containing all nodal loads and nodal displacements respectively. The edge IJ is associated with the axial force it carries, t_{IJ} , and with its percent elongation, e_{IJ} , so that \mathbf{t} and \mathbf{e} , respectively, are the corresponding E -dimensional vectors for the whole framework.

In the linear theory of bar frameworks (Pellegrino and Calladine, 1986), the *equilibrium operator*, \mathbf{A} , a function of \mathbf{p} only, provides the linear relation between axial forces and external loads,

$$\mathbf{A}\mathbf{t} = \mathbf{f}, \quad (1)$$

while its transpose, the *kinematic compatibility operator*, \mathbf{A}^T , links “small” displacements to “small” elongations,

$$\mathbf{A}^T\mathbf{u} = \mathbf{e}.$$

For the purposes of this paper, we consider only the case where the equilibrium operator does not have full rank, meaning that both its nullspace and the nullspace of \mathbf{A}^T are non-empty: there exist *selfstresses*, \mathbf{t}_s , which are balanced by null loads, and *mechanisms*, \mathbf{u}_m , nodal displacements which do not change the length of the edges:

$$\mathbf{A}\mathbf{t}_s = \mathbf{0}, \quad \mathbf{A}^T\mathbf{u}_m = \mathbf{0}.$$

We say that a mechanism is *nontrivial* if it does not correspond to a rigid-body motion of the framework.

2.2 Stiffness and stability

In the linearized theory of elastic frameworks (e.g. see Guest (2006)), the *tangent stiffness operator*, \mathbf{K}_T , provides the linear relation between displacement increments and load increments,

$$\mathbf{K}_T \Delta\mathbf{u} = \Delta\mathbf{f}.$$

This operator is equal to the Hessian of the potential elastic energy with respect to the parameters chosen to identify a configuration. Given an equilibrium configuration satisfying (1), a general stability condition would require \mathbf{K}_T to be positive definite. The tangent stiffness operator can be decomposed as

$$\mathbf{K}_T = \mathbf{K}_M + \mathbf{K}_G,$$

where \mathbf{K}_M is the *material stiffness operator*, which is always positive semidefinite and depends on the elastic stiffness of the edges, and \mathbf{K}_G is the *geometric stiffness operator*, which depends on the

axial forces in the edges. The material stiffness comes into play only when edges change in length; the geometric stiffness comes into play only when edges change in direction.

For tensegrity systems, there are two typical notions of stability. Consider a framework whose equilibrium matrix does not have full rank, and it is subjected to no external forces. We have that $\mathbf{K}_M \mathbf{u} = \mathbf{0}$ if and only if \mathbf{u} is a mechanism, i.e. when edges do not change in length. We say that this framework is *prestress-stable* if it admits a selfstress for which

$$\mathbf{K}_G \mathbf{u}_m \cdot \mathbf{u}_m > 0, \quad \text{for each nontrivial mechanism } \mathbf{u}_m.$$

If the opposite inequality holds for some mechanism, we say that the system is *prestress-unstable*.

Prestress-stability does not imply stability: even if the prestress-stability condition is satisfied, it might happen that there are some \mathbf{u} , which are not mechanisms, for which $\mathbf{K}_T \mathbf{u} \cdot \mathbf{u} < 0$, necessarily having $\mathbf{K}_G \mathbf{u} \cdot \mathbf{u} < 0$, resulting in an unstable system. We say that a tensegrity system is *superstable* if it is prestress-stable and

$$\text{there is no } \mathbf{u} \text{ such that } \mathbf{K}_G \mathbf{u} \cdot \mathbf{u} < 0,$$

so that \mathbf{K}_T must be positive definite. In other words, for a superstable system, the geometric stiffness is positive along nontrivial mechanisms, and nonnegative otherwise.

We see that superstability is a stronger condition than prestress-stability. However, when a framework is prestress-stable, it is always possible to build a corresponding physical structure by making the edges very stiff with respect to the selfstress, or, vice-versa, by applying a very low selfstress with respect to the elastic stiffness of the edges. For this reason, it is usually stated that *a superstable framework is stable independently of the selfstress level and material properties* (Connelly, 1999; Zhang and Ohsaki, 2007).

2.3 Elastic formulations

Each edge is modeled as a linear spring. We associate to each pair of vertices $I, J \in \mathcal{N}$ the scalar k_{IJ} , with $k_{IJ} > 0$ if $IJ \in \mathcal{E}$, and $k_{IJ} = 0$ if $IJ \notin \mathcal{E}$. The axial force of an edge is then given by $t_{IJ} = k_{IJ}(\lambda_{IJ} - \bar{\lambda}_{IJ})$, with λ_{IJ} being the length of the edge, $\lambda_{IJ} = \|\mathbf{p}_J - \mathbf{p}_I\|$, and $\bar{\lambda}_{IJ}$ being the rest length of the corresponding spring. In this way, the elastic energy of the framework is written as

$$U = \frac{1}{2} \sum_{IJ \in \mathcal{E}} k_{IJ} (\lambda_{IJ} - \bar{\lambda}_{IJ})^2.$$

We first consider the case of the configuration \mathbf{p} being a function of n parameters, or Lagrangian coordinates, grouped in the vector $\mathbf{x} \equiv (x_1, \dots, x_n)$. Notice that we use lowercase subscripts for these parameters, not to be confused with the uppercase subscripts employed for nodes and edges. Assuming that no loads are applied to the framework, equilibrium configurations satisfy $\nabla_{\mathbf{x}} U = \mathbf{0}$, where $\nabla_{\mathbf{x}}$ denotes the gradient operator with respect to \mathbf{x} . This is a set of n equations of the form

$$0 = U_{,i} = \sum_{IJ \in \mathcal{E}} k_{IJ} (\lambda_{IJ} - \bar{\lambda}_{IJ}) \lambda_{IJ,i} = \sum_{IJ \in \mathcal{E}} t_{IJ} \lambda_{IJ,i}, \quad i = 1, \dots, n, \quad (2)$$

where $(\cdot)_{,i}$ denotes the partial derivative with respect to x_i . The last expression shows the form of the equilibrium operator, when compared to the compact equation $\mathbf{A} \mathbf{t} = \mathbf{0}$. We see that \mathbf{t} must be a selfstress for the framework. The equilibrium equations are trivially satisfied when $\mathbf{t} = \mathbf{0}$, that is, when the framework is unstressed. This corresponds to having $\lambda_{IJ} = \bar{\lambda}_{IJ}$ for all the edges.

The tangent stiffness operator, $\mathbf{K}_T = \nabla_{\mathbf{x}}^2 U$, can be obtained from (2), we have in components:

$$\begin{aligned} (\mathbf{K}_T)_{ij} = U_{,ij} &= \sum_{IJ \in \mathcal{E}} k_{IJ} \lambda_{IJ,i} \lambda_{IJ,j} + k_{IJ} (\lambda_{IJ} - \bar{\lambda}_{IJ}) \lambda_{IJ,ij} \\ &= \sum_{IJ \in \mathcal{E}} k_{IJ} \lambda_{IJ,i} \lambda_{IJ,j} + t_{IJ} \lambda_{IJ,ij}, \quad i, j = 1, \dots, n, \end{aligned} \quad (3)$$

where the two terms in the summation contribute respectively to \mathbf{K}_M and \mathbf{K}_G , and $(\cdot)_{,ij}$ denotes the second partial derivative with respect to x_i and x_j .

We see that $\mathbf{K}_G = \mathbf{0}$ when the framework is unstressed. To see that \mathbf{K}_M is positive semidefinite, it is enough to consider the framework unstressed, so that $U = 0$. Since U cannot be negative, energy variations can only be positive. Since the first variation is null, $\nabla_{\mathbf{x}} U = \mathbf{0}$, the second variation must be nonnegative, which means that \mathbf{K}_M is positive semidefinite. From the first term in (3), we have that \mathbf{K}_M depends on the material properties of the structure through the spring constants, and it is directly related to changes in length of members, being null only for mechanisms. From the second term in (3), we have that \mathbf{K}_G depends directly on the axial forces, a fact which is true even for different choices of the constitutive behavior. Moreover, \mathbf{K}_G is related to changes in direction of members, a fact which we justify below.

As it often happens in numerical models, the configuration \mathbf{p} can just be a function of the Cartesian coordinates of the nodes. If this is the case, the stiffness operators can be expressed as follows. Let \mathbf{W}_{IJ} be the linear operator

$$\mathbf{W}_{IJ} = k_{IJ} \mathbf{n}_{IJ} \otimes \mathbf{n}_{IJ} + \omega_{IJ} (\mathbf{1}_3 - \mathbf{n}_{IJ} \otimes \mathbf{n}_{IJ}), \quad (4)$$

represented by a 3-by-3 matrix. Here, we have introduced: \mathbf{n}_{IJ} , the unit vector parallel to edge IJ , $\mathbf{n}_{IJ} = (\mathbf{p}_J - \mathbf{p}_I)/\lambda_{IJ}$; $\mathbf{1}_3$, the identity in a three-dimensional vector space; the scalar ω_{IJ} , which is the so-called *stress* of edge IJ , given by $\omega_{IJ} = t_{IJ}/\lambda_{IJ}$. The symbol \otimes represents the dyadic product, defined by the relation

$$(\mathbf{a} \otimes \mathbf{b})\mathbf{c} = (\mathbf{b} \cdot \mathbf{c})\mathbf{a},$$

with \mathbf{a} , \mathbf{b} and \mathbf{c} being arbitrary three-dimensional vectors, and the dot indicating the inner product. The tangent stiffness operator is then represented by a $3N$ -by- $3N$ matrix, partitioned into 3-by-3 blocks, with the block in position IJ given by

$$(\mathbf{K}_T)_{IJ} = \begin{cases} \sum_{IH \in \mathcal{E}} \mathbf{W}_{IH}, & I = J, \\ -\mathbf{W}_{IJ}, & I \neq J. \end{cases} \quad (5)$$

The two terms in (4), $k_{IJ} \mathbf{n}_{IJ} \otimes \mathbf{n}_{IJ}$ and $\omega_{IJ} (\mathbf{1}_3 - \mathbf{n}_{IJ} \otimes \mathbf{n}_{IJ})$, contribute respectively to \mathbf{K}_M and \mathbf{K}_G . We remark that, when \mathbf{K}_T is applied to \mathbf{u} , each \mathbf{W}_{IJ} is applied to the displacement vector of either node I or J . Therefore, since $\mathbf{n}_{IJ} \otimes \mathbf{n}_{IJ}$ and $(\mathbf{1}_3 - \mathbf{n}_{IJ} \otimes \mathbf{n}_{IJ})$ project vectors respectively along the direction of the edge IJ and on the plane orthogonal to it, we have that $\mathbf{K}_M \mathbf{u}$ is nonnull when edges change in length, while $\mathbf{K}_G \mathbf{u}$ is nonnull when edges change in direction.

We further observe that (5) can be viewed as the expression of a discrete weighted Laplacian for the underlying graph of the framework (Godsil and Royle, 2001), where weights are not scalar but given by the operators \mathbf{W}_{IJ} 's.

We now discuss some alternative forms of (5). First, (4) can be rewritten as

$$\mathbf{W}_{IJ} = k_{IJ} \frac{\bar{\lambda}_{IJ}}{\lambda_{IJ}} \mathbf{n}_{IJ} \otimes \mathbf{n}_{IJ} + \omega_{IJ} \mathbf{1}_3. \quad (6)$$

This way, \mathbf{K}_T takes the form

$$\mathbf{K}_T = \widetilde{\mathbf{K}}_M + \widetilde{\mathbf{K}}_G, \quad (7)$$

with $\widetilde{\mathbf{K}}_M$ and $\widetilde{\mathbf{K}}_G$ obtained according to (5) from the contribution of the first and second term of (6) respectively. Notice that $\widetilde{\mathbf{K}}_M$ can be seen as the material stiffness operator of a fictitious elastic framework whose spring constants have the form $\widetilde{k}_{IJ} = k_{IJ} \bar{\lambda}_{IJ} / \lambda_{IJ}$. The operator $\widetilde{\mathbf{K}}_G$ is related to the so-called *stress matrix*, $\boldsymbol{\Omega}$, an N -by- N matrix, defined component-wise as

$$(\boldsymbol{\Omega})_{IJ} = \begin{cases} \sum_{IH \in \mathcal{E}} \omega_{IH}, & I = J, \\ -\omega_{IJ}, & I \neq J. \end{cases} \quad (8)$$

This is actually a standard weighted Laplacian of the underlying graph, with the stresses as scalar weights.

For stiff frameworks, i.e. $\lambda_{IJ} \simeq \bar{\lambda}_{IJ}$ for every edge IJ , we have that

$$\widetilde{\mathbf{K}}_M \simeq \mathbf{K}_M, \quad \widetilde{\mathbf{K}}_G \simeq \mathbf{K}_G.$$

Sometimes in the literature the tangent stiffness operator is computed as

$$\widehat{\mathbf{K}}_T = \mathbf{K}_M + \widetilde{\mathbf{K}}_G,$$

which corresponds to replacing the \mathbf{W}_{IJ} 's with

$$\widehat{\mathbf{W}}_{IJ} = k_{IJ} \mathbf{n}_{IJ} \otimes \mathbf{n}_{IJ} + \omega_{IJ} \mathbf{1}_3.$$

This is probably done to simplify formulas; however, the approximation made is seldom stated explicitly. It is easy to see that, for a mechanism \mathbf{u}_m , $\mathbf{K}_G \mathbf{u}_m = \widetilde{\mathbf{K}}_G \mathbf{u}_m$, so that the prestress-stability condition can be given in term of $\widetilde{\mathbf{K}}_G$ in the same way as before. The definition for superstability usually found in the literature is given in term of the stress matrix, by requiring $\boldsymbol{\Omega}$ to be positive semidefinite, with the dimension of its nullspace equal to four, plus an additional condition (Connelly, 1999). Notice that this corresponds to having a positive semidefinite $\widetilde{\mathbf{K}}_G$, with the dimension of its nullspace equal to twelve. This condition guarantees the framework to be stable only if $\widetilde{\mathbf{K}}_M$ is positive semidefinite, which is true only if $\bar{\lambda}_{IJ} > 0$ for every edge IJ (Guest, 2006). In general, it is possible to have springs with negative rest lengths, e.g. prestressed springs (Guest, 2011). In such case, this definition of superstability does not imply overall stability. The definition of superstability given in Subsection 2.2 is consistent even if prestressed springs are employed. We conclude this section by observing that, no matter which definition is adopted, if we allow for negative rest-lengths, then a prestress-stable system which is not superstable can always become unstable for sufficiently small values of the rest-lengths, i.e. for sufficiently large selfstress. The structure we analyze in the next section is an example where this happens even for positive rest-lengths.

3 The bistable system

The tensegrity system object of this paper is depicted in Fig. 2. The figure on the left shows a *high-symmetry* equilibrium configuration for this system. High-symmetry configurations are prestress-stable only for some choices of the geometric parameters. In such case, there are two possibilities: for low levels of selfstress the equilibrium configuration is stable, and it is unique; for high levels of selfstress the configuration is unstable, and there are two more equilibrium configurations which are stable. These are *low-symmetry* configurations, one of which is shown in Fig. 2 (right). When the high-symmetry configuration is prestress-unstable, the system still possesses two additional stable, low-symmetry, equilibrium configurations.

These constitute the two bistable regimes which are available to this structure. In the following, we first analyze high-symmetry configurations to determine whether they are prestress-stable or not. Then, we construct a reduced-order model for low-symmetry configurations, to look at the energy landscapes in each of the above cases. Finally, we confirm the result of the reduced-order model with a full-order finite-element numerical model.

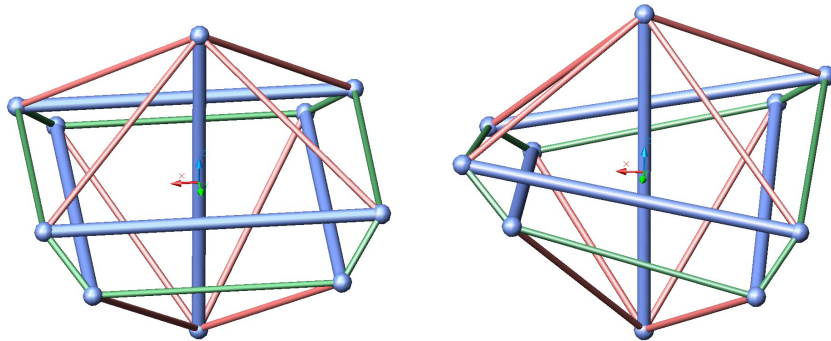


Figure 2: Computer drawings of the bistable system studied in this paper. A high-symmetry configuration (left) and a low-symmetry one (right).

3.1 High-symmetry configurations

We remark that in our analysis we consider the structure as a conventional bar-framework, we use the terms *bar* and *cable* only as labels for the edges of the framework. We check *a posteriori* that the stress in cables is always non-negative in the configurations considered.

Parallel views of a high-symmetry configuration are shown in Fig. 3. The system is composed of five bars and sixteen cables. One bar of length $2H$ is placed on a central vertical axis. Two bars of length $2L$ are placed on the two opposite edges of a horizontal rectangle, while two cables of length $2l$, with $l < L$, form the other two edges of that rectangle. The plane of the rectangle intersects the vertical bar at a distance $h < H$ from the midpoint of the bar. Four cables connect the closer end-node of the vertical bar to the nodes at the vertices of the rectangle. There is another rectangle, identical to the previous one but rotated by an angle of $\pi/2$ about the central vertical axis, placed at the same distance h from the mid-point of the vertical bar, but on the opposite side. Four cables connect the other end-node of the vertical bar to the nodes at the vertices of the latter rectangle. Finally, four more cables connect the end-nodes of the horizontal bars which are closer to each other.

Given the ratio h/H , the ratio l/L is determined by the self-equilibrium conditions when horizontal cables have null stress; we have

$$\frac{l}{L} = \frac{1 - \frac{h}{H}}{1 + \frac{h}{H}}.$$

For each choice of the geometric parameters satisfying this condition, we can construct the equilibrium operator, \mathbf{A} , and verify that it is rank-deficient, thus admitting self-stresses and mechanisms. We find that there is only one independent self-stress state \mathbf{t}_s . With this, we can compute the geometric stiffness operator \mathbf{K}_G and test it for prestress-stability. In this way, we constructed the prestress-stable region for high-symmetry configurations shown in Fig. 4. Later, we will examine two cases, represented by points A and B on this plot.

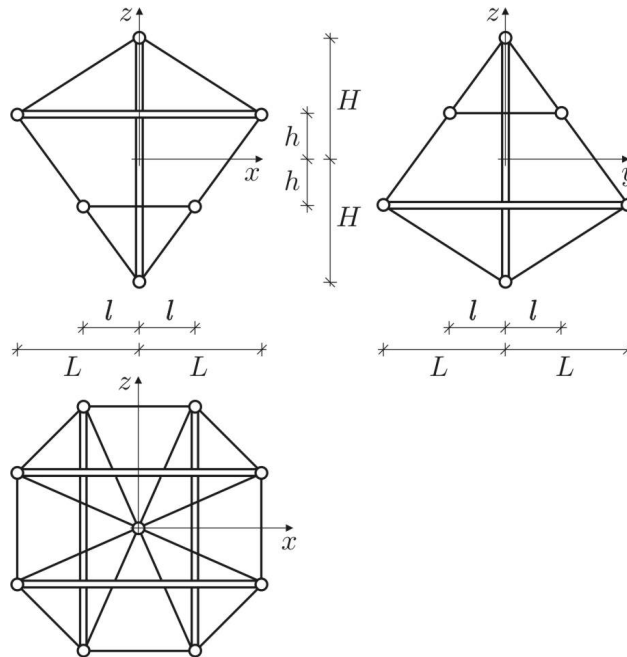


Figure 3: Geometry of the high-symmetry configuration.

3.2 Low-symmetry configurations, reduced-order model

We define low-symmetry configurations as those which remain unchanged under the following symmetry operations (Fig. 5): a rotation of π about the axis z ; an improper rotation of $\pi/2$ about the axis z , that is, a rotation of $\pi/2$ about the axis z plus a reflection with respect to the plane $x - y$. To remove rigid-body motions, we require the vertical bar to remain fixed and parallel to the axis z , while the other bars remain parallel to the coordinate planes $x - z$, $y - z$ (Fig. 5).

If bars are rigid, the number of parameters necessary for identifying each configuration is four. These can be chosen as the three coordinates, x_C, y_C, z_C , of the center C of a horizontal bar, say AB , plus the angle φ between this bar and the horizontal plane, as shown in Fig. 5. With this choice, the expressions of nodal coordinates are reported in Table 1.

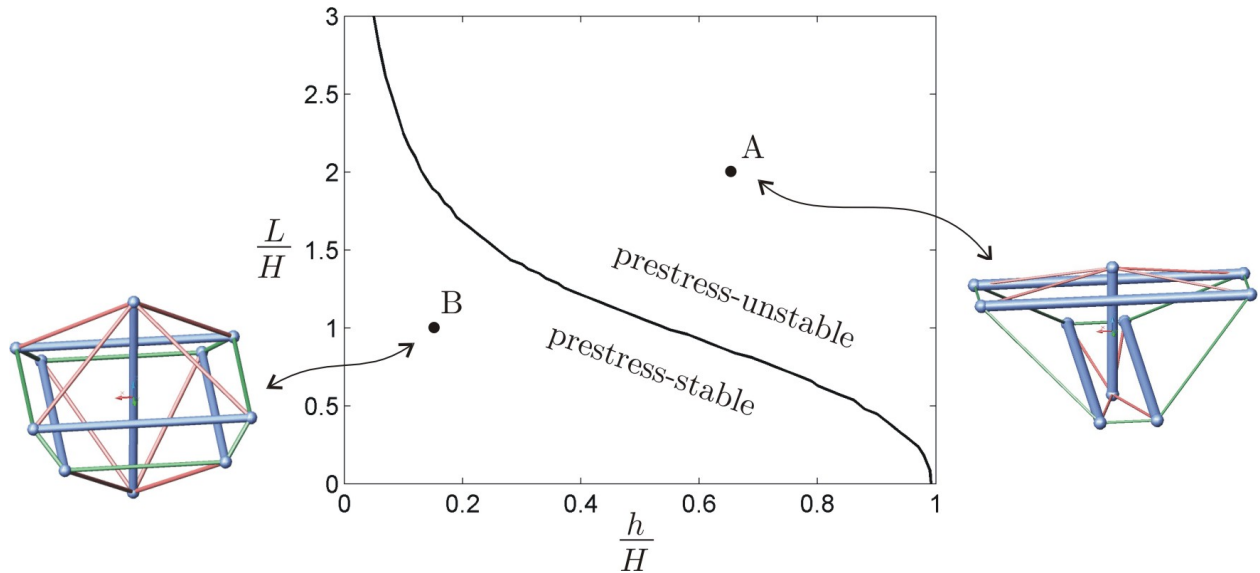


Figure 4: Prestress-stable region. Points A and B identify two particular configurations, which are examined in Section 3.3.

Notice that high-symmetry configurations are obtained for the following values of the parameters:

$$x_C = 0, \quad y_C = l, \quad z_C = h, \quad \varphi = 0. \quad (9)$$

In our model, we consider only eight cables to be linearly elastic, while the other members are inextensible cables and rigid bars. The elastic cables are those labeled as a and b in Fig. 5, plus those symmetrically placed. These cables are depicted in red in Fig. 2. This assumption reduces the number of independent parameters to two, due to the additional constraints given by the inextensibility of cables d and e . The lengths l_d and l_e of these cables, are given by

$$l_d^2 := \|A - B''\|^2 = (x_C - y_C + L \cos \varphi)^2 + (-x_C - y_C + L \cos \varphi)^2 + 4z_C^2, \quad (10)$$

$$l_e^2 := \|B'' - A'''\|^2 = 4y_C^2 + 4x_C^2 + 4L^2(\sin \varphi)^2. \quad (11)$$

node	x	y	z
A	$x_C + L \cos \varphi$	$-y_C$	$z_C + L \sin \varphi$
B	$x_C - L \cos \varphi$	$-y_C$	$z_C - L \sin \varphi$
A'	$-x_C - L \cos \varphi$	y_C	$z_C + L \sin \varphi$
B'	$-x_C + L \cos \varphi$	y_C	$z_C - L \sin \varphi$
A''	y_C	$x_C + L \cos \varphi$	$-z_C - L \sin \varphi$
B''	y_C	$x_C - L \cos \varphi$	$-z_C + L \sin \varphi$
A'''	$-y_C$	$-x_C - L \cos \varphi$	$-z_C - L \sin \varphi$
B'''	$-y_C$	$-x_C + L \cos \varphi$	$-z_C + L \sin \varphi$

Table 1: Nodal coordinates of low-symmetry configurations (see Fig. 5).

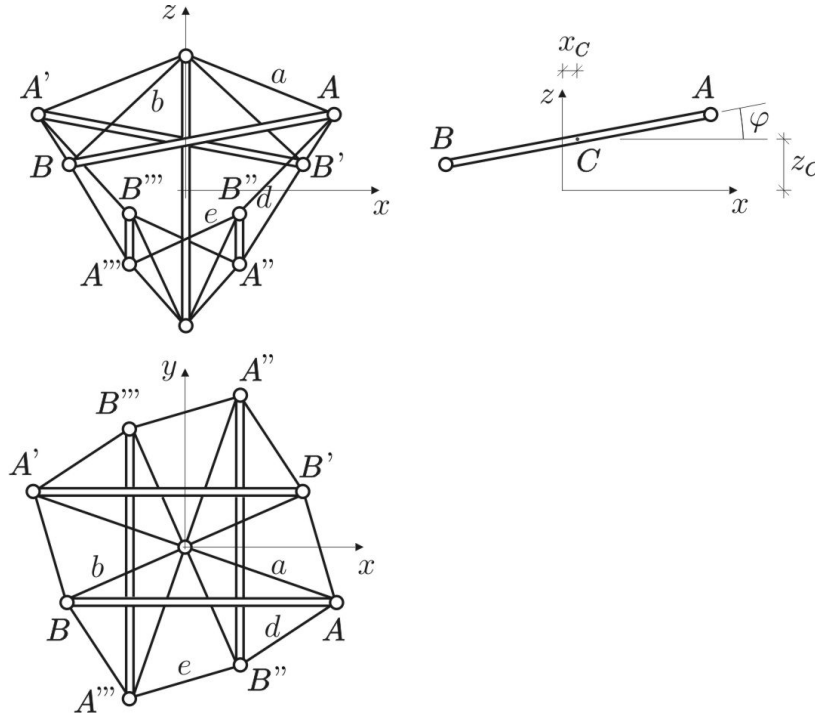


Figure 5: Lagrangian coordinates for the low-symmetry configuration.

By taking φ and x_C as independent parameters, we can solve (10) and (11) for y_C and z_C ,

$$l_d, l_e = \text{const} \quad \Rightarrow \quad y_C = \tilde{y}_C(x_C, \varphi) \quad , \quad z_C = \tilde{z}_C(x_C, \varphi) ,$$

with \tilde{y}_C and \tilde{z}_C expressed as

$$\tilde{y}_C = \sqrt{\frac{1}{4}l_e^2 - x_C^2 - L^2(\sin \varphi)^2} ,$$

$$\tilde{z}_C = \frac{1}{2} \sqrt{l_d^2 - (x_C - \tilde{y}_C + L \cos \varphi)^2 - (-x_C - \tilde{y}_C + L \cos \varphi)^2} .$$

Differentiating (10) and (11), we have:

$$2l_d dl_d = 2(x_C - y_C + L \cos \varphi)(dx_C - dy_C - L \sin \varphi d\varphi) +$$

$$+ 2(-x_C - y_C + L \cos \varphi)(-dx_C - dy_C - L \sin \varphi d\varphi) + 8z_C dz_C ,$$

$$2l_e dl_e = 8y_C dy_C + 8x_C dx_C + 8L^2 \sin \varphi \cos \varphi d\varphi .$$

By substituting the high-symmetry values (9) into these expressions and considering that $dl_d = dl_e = 0$, we obtain:

$$0 = -4(L - l) dy_C + 8h dz_C ,$$

$$0 = 8l dy_C .$$

Then $dy_C = dz_C = 0$ holds in a high-symmetry configuration, which means that small displacements from this configuration occur only with variations in x_C and φ .

The lengths of the elastic cables are expressed by:

$$\lambda_a^2(x_C, \varphi) = \|A - D\|^2 = (x_C + L \cos \varphi)^2 + \tilde{y}_C^2 + (H - \tilde{z}_C - L \sin \varphi)^2,$$

$$\lambda_b^2(x_C, \varphi) = \|B - D\|^2 = (x_C - L \cos \varphi)^2 + \tilde{y}_C^2 + (H - \tilde{z}_C + L \sin \varphi)^2.$$

We will denote by λ_0 the common value of these lengths at high-symmetry configurations, $\lambda_0 = \lambda_a(0, 0) = \lambda_b(0, 0)$.

By differentiating the above expressions at high-symmetry configurations, we can look for the displacements causing null elongations, which correspond to the mechanism. Considering the first expression, we have

$$2\lambda_a d\lambda_a = 2L dx_C + 2l dy_C + 2(H - h)(-dz_C - L d\varphi),$$

and by setting $d\lambda_a = 0$ and $dy_C = dz_C = 0$, we find

$$dx_C = (H - h) d\varphi. \quad (12)$$

Since similar computations for λ_b give the same result, high-symmetry configurations possess a mechanism and its direction is given by (12).

At this point we can compute the potential elastic energy for given rest-lengths and elastic constants of cables a and b :

$$\mathcal{E}_{\text{el}}(x_C, \varphi) = 4 \left(\frac{1}{2} \left(k_a (\lambda_a - \bar{\lambda}_a)^2 + k_b (\lambda_b - \bar{\lambda}_b)^2 \right) \right).$$

3.3 Examples

In the following, we assume same spring constants, $k_a = k_b = k$, and same natural lengths, $\bar{\lambda}_a = \bar{\lambda}_b = \bar{\lambda}$, for the elastic cables. We give examples whose geometric parameters correspond to points A and B in the two different regions shown in Fig. 4:

- **Case A:** a prestress-unstable system with $L = 1$, $H = 1/2$, and $h/H = 0.65$. The elastic constant k is equal to 10, while the ratio $(\lambda_0 - \bar{\lambda})/\lambda_0$ is equal to 0.1.
- **Case B:** a prestress-stable system with $L = 1/2$, $H = 1/2$, and $h/H = 0.15$. The elastic constant is the same as in case A, $k = 10$.
We further consider two situations: $(\lambda_0 - \bar{\lambda})/\lambda_0 = 0.1$ (**Case B1**) and $(\lambda_0 - \bar{\lambda})/\lambda_0 = 0.3$ (**Case B2**).

Figures 6, 7 and 8 show the energy contour plots for cases A, B1 and B2 respectively. In Case A, the system is bistable, with the high-symmetry configuration being unstable. The two stable configurations are placed along the direction of the mechanism, represented by a thick blue line. In Case B1, there is one stable configuration, which is the high-symmetry configuration. In Case B2, the system is bistable. Again the high-symmetry configuration is unstable. The two stable configurations are placed far away from the direction of the mechanism.

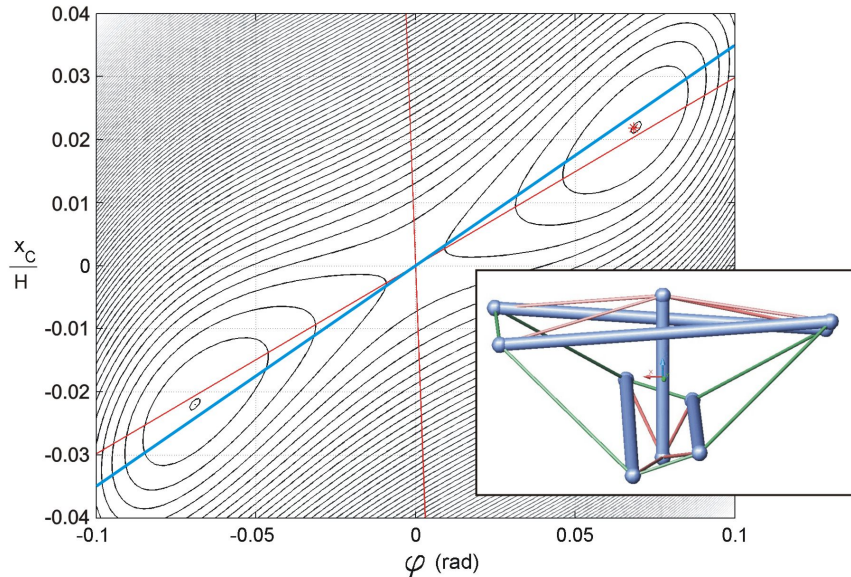


Figure 6: Energy contour plot for Case A: $L/H = 2$, $h/H = 0.65$, $(\lambda_0 - \bar{\lambda})/\lambda_0 = 0.1$. The thick blue line represents the direction of the mechanism. The thin red lines represent the directions of the eigenvectors of the tangent stiffness matrix in a finite element model (notice that they do not appear to be orthogonal to each other due to the scaling of the axes). The red mark corresponds to the equilibrium configuration obtained by a dynamic relaxation procedure applied to the finite element model. The energy increases by 0.41% when passing from the minimum value to the value at the origin.

3.4 Numerical models, critical prestrain

To assess the validity of these results, obtained with a reduced model with only two degrees of freedom, we performed some numerical computations on a full finite element model. Rigid bars and inextensible cables have been assigned very large spring constants.

First, we computed the 30-by-30 tangent stiffness matrix in the high-symmetry configuration. This matrix was then reduced to a 2-by-2 matrix by considering only the two displacement vectors which were compatible with our assumptions on symmetry and inextensibility. The thin red lines shown in Figs. 6, 7 and 8 correspond to the directions of the eigenvectors of this reduced tangent stiffness matrix.

In Case A (Fig. 6) the high-symmetry configuration is unstable. The direction of the mechanism, represented by the blue line, is close to the red line corresponding to the negative eigenvalue. This reflects the prestress-instability condition: the curvature of the energy is negative along the blue line. In Case B, the blue line is not close anymore to the red lines. The high-symmetry configuration is prestress-stable both in Case B1 (Fig. 7) and in case B2 (Fig. 8), with the energy having positive curvature along the blue line. However, the eigenvalues of the reduced matrix are both positive only in Case B1. This shows that there is a critical value of the prestrain, $(\lambda_0 - \bar{\lambda})/\lambda_0$, for which one of the eigenvalues becomes negative, with the high-symmetry prestress-stable configuration becoming unstable. Figure 9 shows the contour plot of the critical prestrain obtained numerically.

To verify that the reduced model effectively captures the behavior of a corresponding physi-

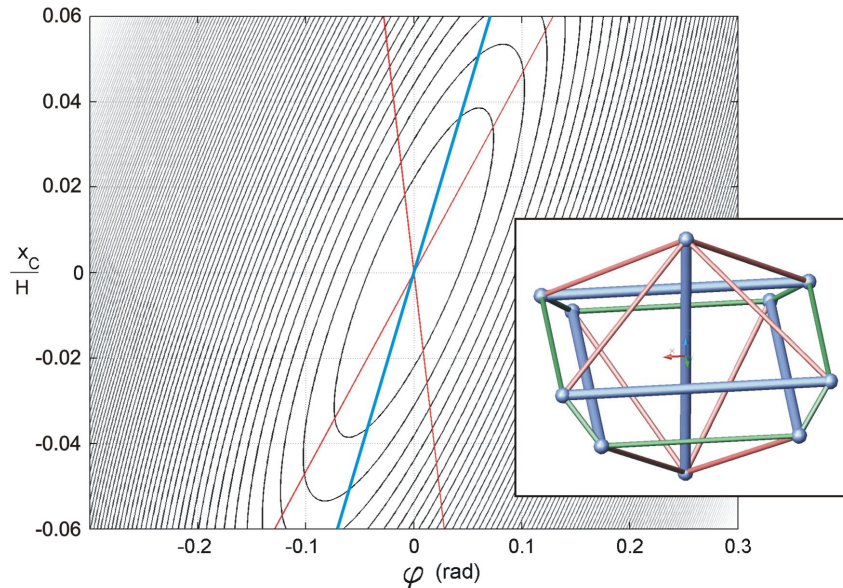


Figure 7: Energy contour plot for Case B1: $L/H = 1$, $h/H = 0.15$, $(\lambda_0 - \bar{\lambda})/\lambda_0 = 0.1$. The thick blue line represents the direction of the mechanism. The thin red lines represent the directions of the eigenvectors of the tangent stiffness matrix in a finite element model (notice that they do not appear to be orthogonal to each other due to the scaling of the axes).

cal system, we applied to the finite element model a dynamic relaxation procedure with kinetic damping. Dynamic relaxation is a form-finding procedure to obtain the equilibrium configuration of tensile-structures and tensegrity structures (Topping and Ivanyi, 2005; Zhang et al., 2006). The equilibrium configurations which have been found by employing this procedure are in agreement with the reduced model. These configurations are marked with a red star in Figs. 6 and 8. Moreover, we verified that the stress in all cables was positive in these configurations.

4 Concluding remarks

This case study showed that it is possible to change the mechanical behavior of a tensegrity system in two different ways. A certain stable system can become unstable, while displaying additional stable configurations, either by changing its geometry, or by increasing its prestress. In the latter situation, the prestress-stable configuration is actually unstable. Usually this can happen when a prestress-stable system is not superstable and we allow the rest-lengths to be negative, as for the case of prestressed springs. In the present system this occurs while rest-lengths remain positive. One open question would be whether additional stable configurations always exist or not, and it can be the subject of further studies.

In relation to this, the definition of superstability given in this paper differs from the one found in the literature, in that it is consistent no matter what is the sign of the rest-lengths: according to our definition, superstability always implies stability.

Regarding the reduced model, the choice of the elastic and inextensible cables is crucial in the analysis. With a different choice we might not be able to catch the bistable behavior. In addition,

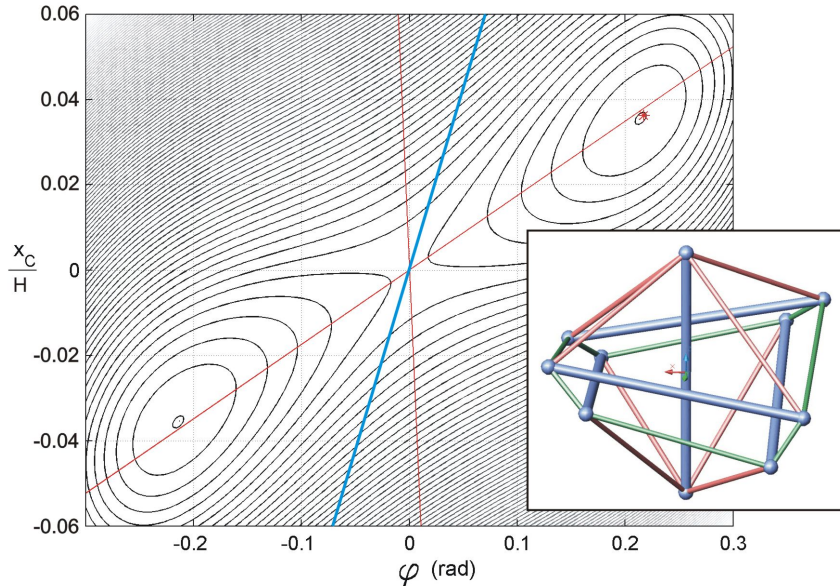


Figure 8: Energy contour plot for Case B2: $L/H = 1$, $h/H = 0.15$, $(\lambda_0 - \bar{\lambda})/\lambda_0 = 0.3$. The thick blue line represents the direction of the mechanism. The thin red lines represent the directions of the eigenvectors of the tangent stiffness matrix in a finite element model (notice that they do not appear to be orthogonal to each other due to the scaling of the axes). The red mark corresponds to the equilibrium configuration obtained by a dynamic relaxation procedure applied to the finite element model. The energy increases by 0.53% when passing from the minimum value to the value at the origin.

in a bistable case, like Case A or Case B2, the energy values at the two minima do not necessarily need to be the same, since different values can be obtained by choosing $k_a \neq k_b$ for the spring constants.

Lastly, every definition of stability given here or in the literature is *local*, i.e. it applies to a particular configuration. Paralleling the definition of global rigidity (Connelly, 2005), we can envisage a notion of *global stability* for elastic systems possessing a unique stable configuration. Globally stable structures are certainly useful in applications. A characterization of global stability would then allow one to distinguish between globally stable systems and multistable ones, such as those already found in the literature.

Acknowledgements

The author would like to thank Simon Guest for providing useful comments on a draft version of this paper. The author would also like to thank Walter Whiteley for bringing up the remark on the choice of the elastic and inextensible cables.

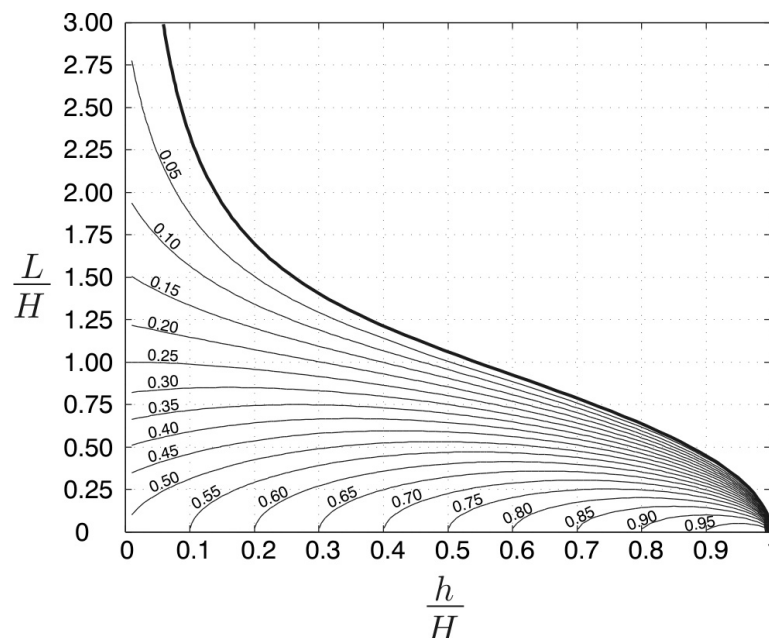


Figure 9: Contour plot of critical prestrain as a function of the geometric parameters. When $(\lambda_0 - \lambda_N)/\lambda_0$ becomes greater than the critical prestrain, the structure becomes bistable. This means that the high-symmetry prestress-stable configuration becomes unstable. The thick line correspond to the boundary between prestress-stable and prestress-unstable regions (*cf* Fig.4). The critical prestrain tends to zero when approaching the boundary.

References

- C. R. Calladine. Buckminster Fuller’s ‘tensegrity’ structures and Clerk Maxwell’s rules for the construction of stiff frames. *International Journal of Solids and Structures*, 14:161–172, 1978. doi: [http://dx.doi.org/10.1016/0020-7683\(78\)90052-5](http://dx.doi.org/10.1016/0020-7683(78)90052-5).
- R. Connelly. Rigidity and energy. *Inventiones Mathematicae*, 66:11–33, 1982. doi: <http://dx.doi.org/10.1007/BF01404753>.
- R. Connelly. Generic global rigidity. *Discrete Computational Geometry*, 33:549–563, 2005. doi: <http://dx.doi.org/10.1007/s00454-004-1124-4>.
- R. Connelly. Tensegrity structures: Why are they stable? In *Rigidity Theory and Applications*, pages 47–54. Kluwer Academic/Plenum Publishers, 1999.
- M. Defosse. Shape memory effect in tensegrity structures. *Mechanics Research Communications*, 30:311–316, 2003. doi: [http://dx.doi.org/10.1016/S0093-6413\(03\)00030-2](http://dx.doi.org/10.1016/S0093-6413(03)00030-2).
- F. Fraternali, L. Senatore, and C. Daraio. Solitary waves on tensegrity lattices. *Journal of the Mechanics and Physics of Solids*, 60(6):1137 – 1144, 2012. ISSN 0022-5096. doi: 10.1016/j.jmps.2012.02.007.
- C. Godsil and G. Royle. *Algebraic Graph Theory*. Springer, 2001.

- V. Gómez Jáuregui. Controversial origins of tensegrity. In Alberto Domingo and Carlos Lazaro, editors, *Proceedings of IASS 2009, Valencia, Spain*, 2009.
- S D Guest. The stiffness of prestressed frameworks: A unifying approach. *International Journal of Solids and Structures*, 43(3–4):842–854, 2006. doi: <http://dx.doi.org/10.1016/j.ijsolstr.2005.03.008>.
- S.D. Guest. The stiffness of tensegrity structures. *IMA Journal of Applied Mathematics*, 76:57–66, 2011. doi: <http://dx.doi.org/10.1093/imamat/hxq065>.
- J. Michielsen, R. H. B. Fey, and H. Nijmeijer. Steady-state dynamics of a 3d tensegrity structure: Simulations and experiments. *International Journal of Solids and Structures*, 49:973–988, 2012. doi: <http://dx.doi.org/10.1016/j.ijsolstr.2011.12.011>.
- K. W. Moored and H. Bart-Smith. Investigation of clustered actuation in tensegrity structures. *International Journal of Solids and Structures*, 46:3272–3281, 2009. doi: <http://dx.doi.org/doi:10.1016/j.ijsolstr.2009.04.026>.
- R. Motro. *Tensegrity: structural systems for the future*. Kogan Page Science, London, U.K., 2003.
- R Motro. Tensegrity systems: The state of the art. *International Journal of Space Structures*, 7 (2):75–83, 1992.
- I. J. Oppenheim and W. O. Williams. Vibration of an elastic tensegrity structure. *European Journal of Mechanics A/ Solids*, 20:1023–1031, 2001. doi: [http://dx.doi.org/10.1016/S0997-7538\(01\)01181-0](http://dx.doi.org/10.1016/S0997-7538(01)01181-0).
- I. J. Oppenheim and W. O. Williams. Tensegrity prisms as adaptive structures. *Adaptive Structures and Material Systems ASME*, 54:113–120, 1997.
- I. J. Oppenheim and W. O. Williams. Geometric effects in an elastic tensegrity structure. *Journal of Elasticity*, 59(1–3):51–65, 2000. doi: <http://dx.doi.org/10.1023/A:1011092811824>.
- C. Paul, H. Lipson, and F. J. Valero Cuevas. Design and control of tensegrity robots for locomotion. *IEEE Transactions on Robotics*, 22(5):944–957, 2005. doi: <http://dx.doi.org/10.1109/TRO.2006.878980>.
- S. Pellegrino and C. R. Calladine. Matrix analysis of statically and kinematically indeterminate frameworks. *International Journal of Solids and Structures*, 22:409–428, 1986. doi: [http://dx.doi.org/10.1016/0020-7683\(86\)90014-4](http://dx.doi.org/10.1016/0020-7683(86)90014-4).
- P. Ranganathan, S. M. Sivakumar, and P.S.Vignesh. Twinning like behaviour in tensional integrity structures. In *Proceedings of ISSS 2005, Bangalore, India*, 2005.
- D. Rastorfer. Structural gymnastic for the olympics. *Architectural Record*, 176:128–135, 1988.
- B. Roth and W. Whiteley. Tensegrity frameworks. *Transactions of the American Mathematical Society*, 265:419–446, 1981. doi: <http://dx.doi.org/10.1090/S0002-9947-1981-0610958-6>.
- M. Shibata and S. Hirai. Rolling locomotion of deformable tensegrity structure. In *Proceedings of CLAWAR 2009, Istanbul, Turkey*, 2009.

- R. E. Skelton and M. C. de Oliveira. *Tensegrity systems*. Springer, 2009.
- R. E. Skelton and C. Sultan. Controllable tensegrity: a new class of smart structures. In *Proceedings of SPIE, Vol. 3039, pp. 166-177*, 1997. doi: <http://dx.doi.org/10.1117/12.276535>.
- B. H. V. Topping and P. Ivanyi. *Computer aided design of cable membrane structures*. Saxe-Coburg Publications, 2005.
- X. Xu and Y. Luo. Form-finding of nonregular tensegrities using a genetic algorithm. *Mechanics Research Communications*, 37:85–91, 2010. doi: <http://dx.doi.org/doi:10.1016/j.mechrescom.2009.09.003>.
- X. Yuan, L. Chen, and S. Dong. Prestress design of cable domes with new forms. *International Journal of Solids and Structures*, 44:2773–2782, 2007. doi: <http://dx.doi.org/10.1016/j.ijsolstr.2006.08.026>.
- J. Y. Zhang and M. Ohsaki. Stability conditions for tensegrity structures. *International Journal of Solids and Structures*, 44:3875–3886, 2007. doi: <http://dx.doi.org/10.1016/j.ijsolstr.2006.10.027>.
- J. Y. Zhang, S. D. Guest, M. Ohsaki, and R. Connelly. Multi-stable star-shaped tensegrity structures. In *Proceedings of IABSE-IASS 2011, London, UK*, 2011.
- L. Zhang, B. Maurin, and R. Motro. Form-finding of nonregular tensegrity systems. *Journal of Structural Engineering*, 132(9):1435–1440, 2006. doi: [http://dx.doi.org/10.1061/\(ASCE\)0733-9445\(2006\)132:9\(1435\)](http://dx.doi.org/10.1061/(ASCE)0733-9445(2006)132:9(1435)).
- V.S. Zolesi, P.L. Ganga, L. Scolamiero, A. Micheletti, P. Podio-Guidugli, A.G. Tibert, A. Donati, and M. Ghiozzi. On an innovative deployment concept for large space structures. In *Proceedings of ICES 2012, San Diego, CA, USA*, 2012. doi: <http://dx.doi.org/10.2514/6.2012-3601>.